Spatial interference encoding patterns based super resolved photoacoustic microscopy

Amihai Meiri[1], Eric M. Strohm[2], Michael C. Kolios[2] and Zeev Zalevsky[1]

[1]Faculty of Engineering and the Nano Technology Center, Bar-llan University, Ramat-Gan, Israel

[2]Department of Physics, Ryerson University, 350 Victoria Street, Toronto, Ontario, Canada

ABSTRACT

Single sensor (pixel) signals require scanning of the sample in order to obtain spatial information. In this paper we show that using interference, optically induced signals can be reconstructed when recorded using interference pattern excitation, rather than a point illumination. This method reduces the need for dense scanning and requires a small number of scans, or can eliminate the need for scanning in some cases. It is shown that this method can be used in particular in photo-acoustic imaging.

Keywords: Speckles, Photoacoustics, Interference

1. INTRODUCTION

Photoacoustic (PA) imaging has been studied in the last two decades to allow imaging with higher penetration depths than purely optical techniques with better resolution than ultrasound imaging. Among these techniques we can mention PA tomography[1,2] and PA microscopy[3–10] . In PA microscopy, a modulated laser induces an acoustic wave that is detected by an acoustic transducer. The sample is then scanned by moving either the focused acoustic transducer, or a focused excitation laser where the sample stage is raster scanned. In both techniques, the scanning is necessary to obtain the spatial features that compose the sample. The PA signal comes from absorption of the optical radiation by the sample, where the contrast results from the different absorption of the investigated agent from the environment.[11] Another option is to use contrast agents that are attached to the sample. These contrast agents exhibit higher absorption than the surrounding media, thus providing higher contrast in the recorded PA signal[12,13]

Here we show that optically induced signals can be encoded using projected spatial interference patterns, eliminating the need for dense raster scanning of the sample, or the scanning altogether. In addition, the projected spatial encoding patterns can be used as in the case of compressed sensing in order to be able to reconstruct the full field of view at high resolution while using smaller number of projected patterns. We show that by using (primary) speckle encoding, the sample can be imaged if the signal is proportional to the electromagnetic field or the intensity of the incident light (as in the case of photoacoustics[14]).

The main advantages of the proposed concept is the fact that the information on the full field of view of the object is obtained directly from using a small number of projected encoding patterns. Increasing the number of the projected patterns further enhances the resolution of the reconstructed image.

2. SPECKLE ENCODING

For this technique we project a random set of speckle patterns that will encode the object. The random speckle pattern generates a signal that originates from positions within the object that correspond to the locations of the spots of light within the projected pattern (constructive interference). The encoding/decoding sequence is as follows:

A speckle pattern is projected onto the sample and a photoacoustic signal is recorded. The speckle pattern changes with respect to the sample, either by moving the diffuser slightly or by stage scanning, and another photoacoustic signal is recorded. This process is repeated N times. To decode, the recorded signal for each speckle pattern is multiplied by a decoding mask and summed for all the different patterns. In the following section we layout the mathematics of the encoding\decoding process and show that if the decoding mask is the speckle pattern that corresponds to each of the photoacoustic recordings, then the reconstruction results in the decoded object.

Photons Plus Ultrasound: Imaging and Sensing 2017, edited by Alexander A. Oraevsky, Lihong V. Wang, Proc. of SPIE Vol. 10064, 1006453 · © 2017 SPIE · CCC code: 1605-7422/17/$18 · doi: 10.1117/12.2251675

2.1 Theory

For the method we use a different speckle pattern each time a photoacoustic signal is recorded. The results of the speckle pattern encoding and the subsequent light induced signal can be written as:

$$F(p,q)=\sum_m\sum_n s_{p,q}(m,n)O(m,n)\ , \tag{1}$$

where $O(m,n)$ is the original light induced signal, and $s_{p,q}(m,n)$ is the speckle pattern, where we used p,q as the index (instead of a single index) for convenience, since the time dependent speckle pattern can be generated using a constant speckle pattern with time dependent position of the object with respect to the speckle (through stage scanning). To reconstruct the object, we have to multiply the resulting signal by the decoding mask, $\tilde{s}_{p,q}(m,n)$, which is the recorded speckle pattern that corresponds to each p,q pair, *i.e.*:

$$R(r,s)=\sum_p\sum_q F(p,q)\tilde{s}_{p,q}(r,s) \tag{2}$$

We substitute Eq. (2) into Eq. (1), and for convenience continue with a 1D signal:

$$\begin{aligned} F(p)&=\sum_m s_p(m)O(m)\\ R(r)&=\sum_p F(p)\tilde{s}_p(r)\\ R(r)&=\sum_p\sum_m s_p(m)O(m)\tilde{s}_p(r) \end{aligned} \tag{3}$$

Changing the order of summation we have:

$$R(r)=\sum_m O(m)\sum_p s_p(m)\tilde{s}_p(r) \tag{4}$$

The summation over the product of the speckle patterns is the autocorrelation. We can write this as:

$$\sum_p s_p(m)\tilde{s}_p(r)=k+\delta(m-r), \tag{5}$$

Thus:

$$R(r)=\sum_m O(m)\delta(m-r)=k\sum_m O(m)+O(r) \tag{6}$$

If the speckle values are randomly distributed with a mean of *0*, then *k=0* and

$$R(r)=O(r). \tag{7}$$

2.2 Results

To validate our method we first ran numerical simulations. For these numerical simulations a random speckle pattern was generated in the following way: Every pixel was assigned with a random phase value between *0* and 2π, $\phi(m,n)$. The speckle pattern was then a Fourier transform of a complex exponential of the phase values, $s(m,n)=F\left\{e^{i\phi(m,n)}\right\}$, where F denotes Fourier transform. In the simulation every recorded frame has a speckle pattern which decodes the object, the k-th frame can be described using Eq. (1). We tested two different cases: (1) The speckle pattern $s_{p,q}$ is independent between subsequent frames, i.e. it is completely random. Here a new random speckle pattern was generated for every signal recording, using the method described above. (2) The speckle pattern $s_{p,q}=s$ is equal for all captured frames, but the object moves with respect to the speckle pattern. Here just one speckle pattern is generated using the method described above. This case corresponds to a moving stage. For this case, Eq. (1) can be re-written as:

$$F(p,q)=\sum_m\sum_n s_{p,q}(m,n)O(m-p\Delta x,n-q\Delta y) \tag{8}$$

For both cases, the object was reconstructed using Eq. (10). For the random speckle pattern case one can choose the decoding pattern, $\tilde{s}_{p,q}(m,n)$, to be the same as the encoding speckle pattern

$$\tilde{s}_{p,q}(m,n)=s_{p,q}(m,n) \tag{9}$$

Moving the stage then:

$$\tilde{s}_{p,q}(m,n) = s(m - p\Delta x, n - q\Delta y). \tag{10}$$

Since moving the stage with respect to the speckles is equivalent to moving the speckles with respect to the stage, we reconstruct the object by applying Eq. (5), *i.e.* moving the speckles.

The simulation results for the independent random speckle patterns can be seen in Figure 1. In this simulation we varied the number of speckle patterns used between 1,000 and 100,000, and also the number of speckles per ring element width (a ring target is used in this example). The results in Figure 1(a)-(d) show that for 10,000 speckle pattern images, all sampling densities can resolve the ring shape. As the sampling density decreases, the results improve due to averaging. When using 100,000 random speckle patterns, the results, shown in Figure 1(e)-(h), are noticeably better than for the case of 10,000 random speckle patterns. The improvement with reduced sampling density is apparent.

To quantify our results, we measured the contrast in each of the images. To calculate the contrast, we calculated the mean values of the reconstructed image, where the ring target was set to 1, and the mean value of the reconstructed image, where the ring target was 0, and divided the two values, i.e.:

$$C = \frac{\sum_r \sum_s R(r,s)\Big|_{O(r,s)=1}}{\sum_r \sum_s R(r,s)\Big|_{O(r,s)=0}} \tag{11}$$

The results for all the cases can be seen in Figure 1(i). As the number of speckle patterns increases, the contrast improves. We can also see that the lower the sampling density is, the better the results.

For the second case, where the speckle pattern was constant and the stage moved, we see in Figure 2 that when the sampling density is higher, the results are better. This is opposite to the previous simulation and can be explained by the fact that the sampling density also determines the scanning step. With higher sampling density, the scanning step for the sample was smaller, i.e. finer stepping. In this simulation we also calculated the contrast, which supports this statement.

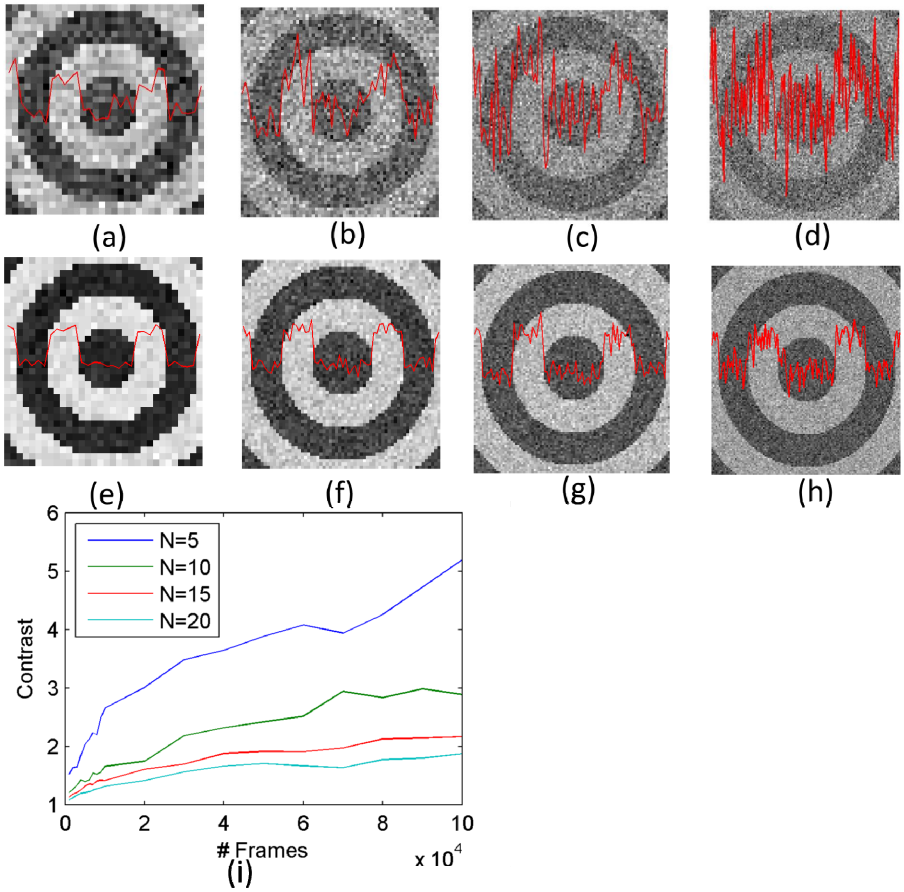

Figure 1. Simulation of ring pattern images using random speckle patterns to spatially encode.: (a)-(d) for 10,000 random speckle patterns with sampling density of (a) 5, (b) 10 (c) 15, and (d) 20 speckles per ring line width. (e)-(h) for 100,000 random speckle patterns with sampling density of (e) 5, (f) 10 (g) 15, and (h) 20 speckles per ring line width. (i) The contrast as a function of number of random speckle patterns for different sampling densities.

In photo-acoustic microscopy[14], the recorded signal is:

$$O(r) = \frac{-if\beta}{2C_p r} AIe^{2\pi ifr/v_s} \tag{12}$$

where f is the temporal modulation frequency, β is the thermal expansion coefficient, C_p is the specific heat, v_s is the speed of sound in the surrounding medium, AI is the absorbed light intensity, and r is the distance from the object absorbing the light and generating the acoustic signal to the detector. We can see that in this case, the signal is proportional to the intensity of the light.

Revisiting Eq. (5), using Eq. (9), we notice that if the speckle pattern can have positive values only, the constant k is not 0. Also, we notice that in practical situations the speckle pattern is constrained in space:

$$S_p(x) = S_p^{(i)}(x)rect(x/D), \tag{13}$$

where D is the size of the window and $S_p^{(i)}(x)$ is an infinite (i.e. not constrained in space) speckle pattern. For this case, the auto-correlation generates a triangle shape added to a delta function, rather than a constant (compare Figure 3(a) and Figure 3(b)). This renders the reconstruction difficult. To overcome this, we duplicate the speckle pattern in the reconstruction in a way that:

$$\tilde{s}_p(m) = s_p(m-D) + s_p(m) + s_p(m+D). \tag{14}$$

A correlation of the duplicated speckle pattern and the original speckle pattern can be seen in Figure 3(c). Now the auto-correlation is composed of 3 delta functions. Taking only the central part will result in Eq. (13) and the image can be reconstructed.

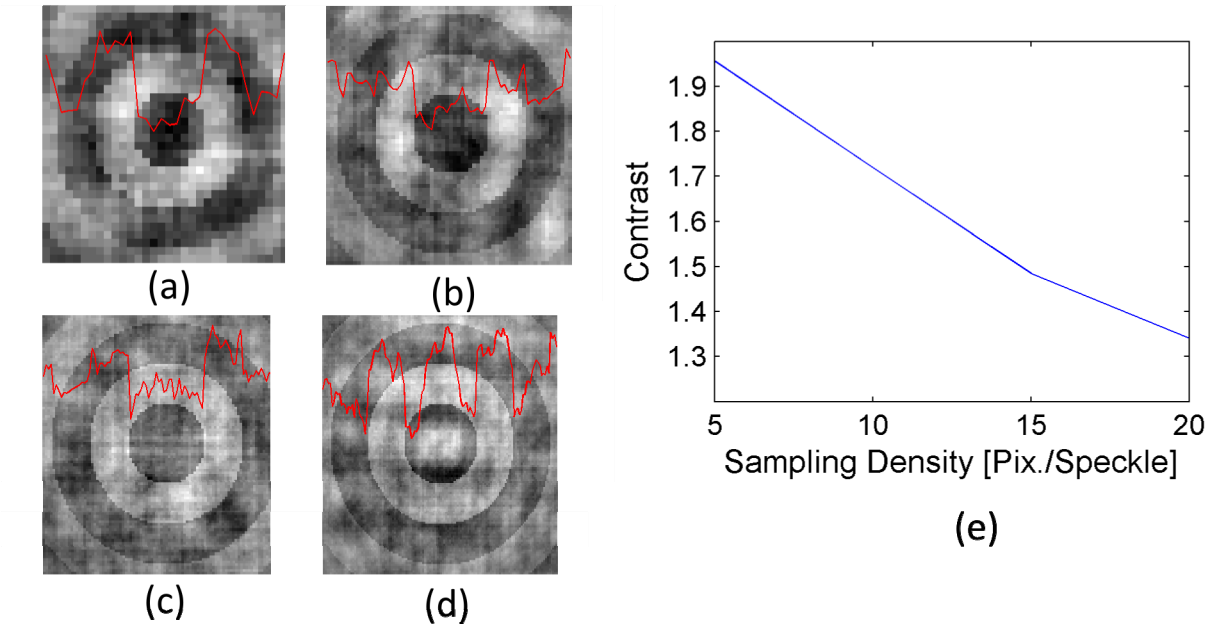

Figure 2. Simulations of a moving stage scanning. The sampling density is (a) 5, (b) 10 (c) 15, and (d) 20 speckles per ring line width. (e) The contrast of the reconstructed image as a function of sampling density.

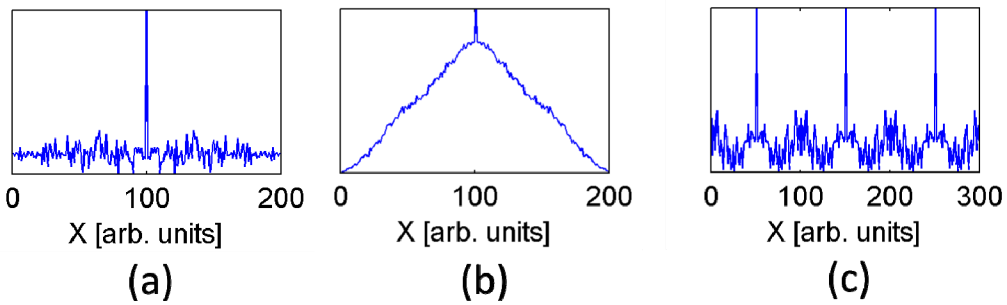

Figure 3. Correlation of speckle patterns. (a) Auto-correlation for a speckle pattern where the speckle pattern can have positive and negative values (signal proportional to the light electric field.) (b) Auto-correlation for a speckle pattern where the speckle pattern can have positive values only (signal proportional to the light intensity.) (c) Correlation between the speckle pattern and 3 duplicates of the speckle pattern, for a speckle pattern where the speckle pattern can have positive values only (signal proportional to the light intensity).

To test the ability to use the method when the signal is proportional to the light intensity we ran the simulations, where this time Eq. (14) applies. In this case, we only used the stage scanning (or speckle scanning) method. The results of the simulation can be seen in Figure 4, where the sampling density was varied between 1 and 20. The results for sampling densities of 1,5,10 and 20 speckles per line are shown in Figure 4(a)-(d), respectively. The contrast as a function of sampling density can be seen in Figure 4(e). The results show that the smaller the number of speckles per line, the better is the contrast.

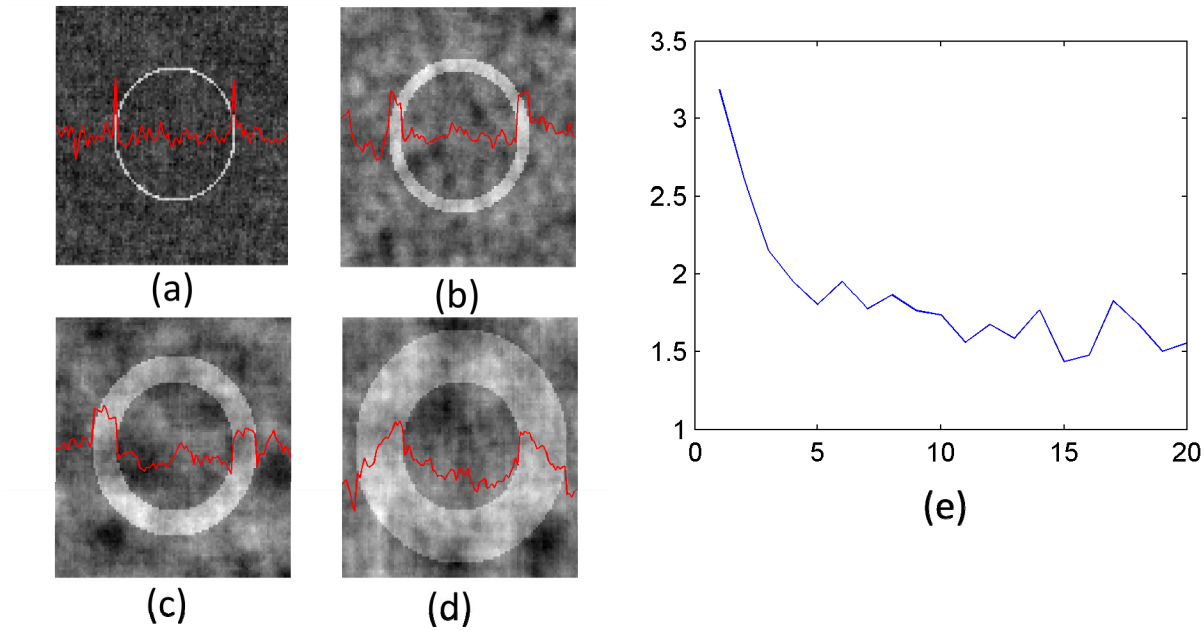

Figure 4. Simulations of a moving stage scanning. The sampling density is (a) 1, (b) 5 (c) 10, and (d) 20 speckles per ring line width. (e) The contrast of the reconstructed image as a function of sampling density.

2.3 Simulating photoacoustic signal using experimentally acquired speckles

Experimentally we used a 532 nm laser which was directed towards the sample through the side port of an Olympus IX81 microscope using a 10x objective. For the sample, we used $1\mu m$ black polystyrene microspheres (Polysciences Inc., USA). We then attached a diffuser to the input port of the microscope and recorded the speckle pattern (see Figure 5(b)) using a Lumenera lu165m camera with a pixel size of 6.45μm. We digitally reversed and used thresholding on the bead image to remove the noise resulting in the camera (simulating an environment where only the bead shows photoacoustic response). We then generated a photoacoustic signal using the stage scanning method by digitally applying see, Eq. (10). We then used the same speckle pattern for the reconstruction as described earlier.

At first, we used a simulated speckle pattern as in the simulations. To compare the reconstruction with the original target, we subtracted the mean value of the reconstructed image to eliminate the background, and set the negative values to 0. The results of the reconstruction overlaid over the original bead target can be seen in Figure 5(a),(e). We see that the simulated speckles resulted in accurate reconstruction of the target. We then used the experimental speckle pattern in Figure 5(b),(f). The results can be seen in Figure 5(c),(g). In this case, the target was not well reconstructed and the resulting shape was round (see inset). This leads to the conclusion that the particular speckle pattern cannot resolve shape as small as our bead. To verify that, we used the same bead image, this time digitally magnified by a factor of 2. This is equivalent to reducing the size of the speckles relative to the target. The reconstruction in this case, in Figure 5(d) is more accurate, which verifies our conclusion.

This phenomena can be described by means of a similar to a Point-Spread-Function (PSF) of a microscope, where structures smaller than the diffraction limit cannot be resolved, thus when imaging small object, the resulting shapes takes the form of the PSF. The PSF of this imaging method can be seen in the inset of Figure 5(c), where larger objects can be resolved.

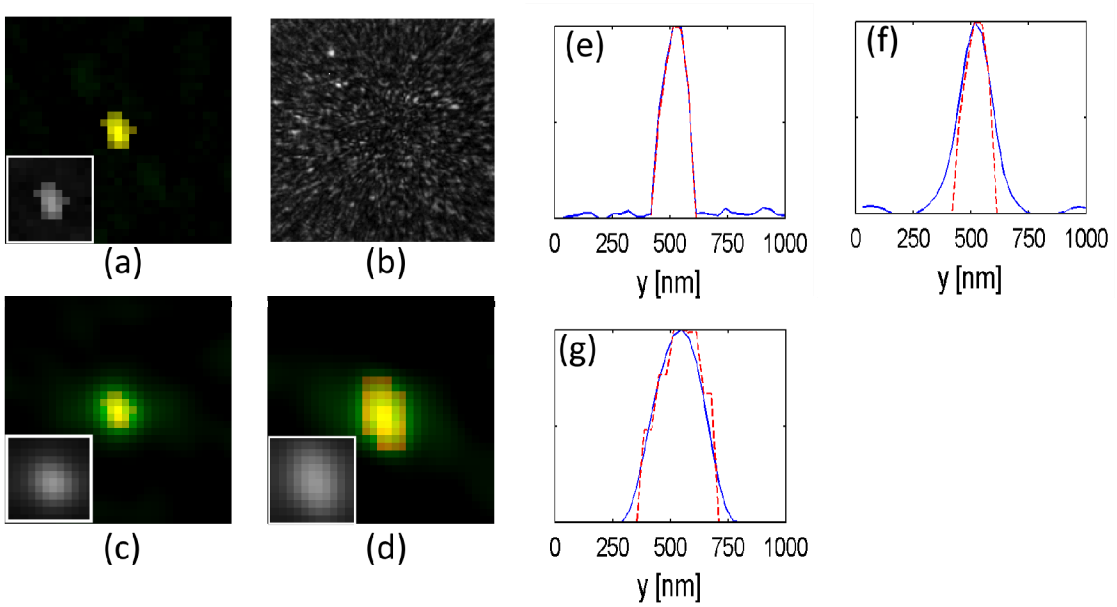

Figure 5. Experimental bead image reconstruction. (a) The bead with simulated speckles. (b) Experimental speckle pattern. (c) The bead with experimental speckles. (d) The bead digitally magnified with experimental speckles. In (a), (c), (d) The reconstruction is in green, the target is in red. The overlap between the target and the reconstruction is in yellow. Inset at bottom left: The original target for each case. (e),(f),(g) the vertical cross section of the target (red) and reconstruction (blue) for (a),(c),(d) respectively.

3. CONCLUSIONS

In this paper we showed that speckle encoding can be used in order to resolve a sample using light-induced signals that are proportional either to the electromagnetic field or the intensity of the incident light. This technique uses sparse scanning of the sample.

The proposed system requires a simple diffuser in order to generate the speckle patterns, where a specially designed phase element can improve the results. The design of such an element is the subject of future research. The placement of the phase element is simple and does not require a complicated system or alignment process. The sample stage also does not require high accuracy, as long as the speckles in the different positions/patterns eventually cover the entire field of view. The decoding of the image requires simple correlation calculation that does not consume high processing complexity.

REFERENCES

[1] Wang, X., Pang, Y., Ku, G., Xie, X., Stoica, G.., Wang, L. V., "Noninvasive laser-induced photoacoustic tomography for structural and functional in vivo imaging of the brain," Nat. Biotechnol. **21**(7), 803–806 (2003).

[2] Wang, L. V.., Hu, S., "Photoacoustic Tomography: In Vivo Imaging from Organelles to Organs," Science **335**(6075), 1458–1462 (2012).

[3] Rosencwaig, A.., Busse, G., "High-resolution photoacoustic thermal-wave microscopy," Appl. Phys. Lett. **36**(9), 725–727 (1980).

[4] Zhang, H. F., Maslov, K., Stoica, G.., Wang, L. V., "Functional photoacoustic microscopy for high-resolution and noninvasive in vivo imaging," Nat. Biotechnol. **24**(7), 848–851 (2006).

[5] Wang, L. V., "Multiscale photoacoustic microscopy and computed tomography," Nat. Photonics **3**(9), 503–509 (2009).

[6] Maslov, K., Zhang, H. F., Hu, S.., Wang, L. V., "Optical-resolution photoacoustic microscopy for in vivo imaging of single capillaries," Opt. Lett. **33**(9), 929 (2008).

[7] Maslov, K., Stoica, G.., Wang, L. V., "In vivo dark-field reflection-mode photoacoustic microscopy," Opt. Lett. **30**(6), 625 (2005).
[8] Zhang, H. F., Maslov, K.., Wang, L. V., "In vivo imaging of subcutaneous structures using functional photoacoustic microscopy," Nat. Protoc. **2**(4), 797–804 (2007).
[9] Favazza, C. P., Jassim, O., Cornelius, L. A.., Wang, L. V., "In vivo photoacoustic microscopy of human cutaneous microvasculature and a nevus," J. Biomed. Opt. **16**(1), 16015–16015 (2011).
[10] Xie, Z., Jiao, S., Zhang, H. F.., Puliafito, C. A., "Laser-scanning optical-resolution photoacoustic microscopy," Opt. Lett. **34**(12), 1771–1773 (2009).
[11] Xu, M.., Wang, L. V., "Photoacoustic imaging in biomedicine," Rev. Sci. Instrum. **77**(4), 41101 (2006).
[12] Luke, G. P., Yeager, D.., Emelianov, S. Y., "Biomedical applications of photoacoustic imaging with exogenous contrast agents," Ann. Biomed. Eng. **40**(2), 422–437 (2012).
[13] Yang, X., Stein, E. W., Ashkenazi, S.., Wang, L. V., "Nanoparticles for photoacoustic imaging," Wiley Interdiscip. Rev. Nanomed. Nanobiotechnol. **1**(4), 360–368 (2009).
[14] Winkler, A. M., Maslov, K.., Wang, L. V., "Noise-equivalent sensitivity of photoacoustics," J. Biomed. Opt. **18**(9), 97003–97003 (2013).